Electronic Supplementary Information

Cocrystal trimorphism as a consequence of orthogonality of halogen- and hydrogen-bonds synthons

Filip Topić, Katarina Lisac, Mihails Arhangelskis, Kari Rissanen*, Dominik Cinčić* and Tomislav Friščić*

Table of Contents

1. Experimental details

All solvents used for syntheses and crystal growth were of reagent grade and were used as received. Methyldiphenylphosphine oxide (**mdppo**), *N*,*N'*-dimethylthiourea, octafluoro-1,4-diiodobutane (**ofib**) and pentafluoroiodobenzene were purchased from Sigma-Aldrich, while tetrafluoro-1,4-diiodobenzene (**tfib**) was purchased from Oakwood Products, Inc.

Mechanochemical experiments were conducted on a Retsch MM200 mill operating at 25 Hz frequency using a 14 mL polytetrafluoroethylene (PTFE) jar along with a zirconia ball (10 mm diameter and 4 g weight).

Powder X-ray diffraction (PXRD) experiments were performed on a Bruker D8 Advance diffractometer with CuKα (1.54184 Å) radiation source operating at 40 mA and 40 kV, equipped with a Lynxeye XE linear position sensitive detector, in the 2θ range of 3−40°, step size of 0.02° and measuring time of 0.5 s per step.

Thermal Analysis. Simultaneous TGA and DSC measurements were performed using a Mettler-Toledo TGA/DSC 1 thermal analyzer in open alumina crucibles (70 μL), heated in a stream of nitrogen (50 mL min^{-1}) at a heating rate of 5 °C min^{-1} up to 150 °C and a heating rate of 10 °C min^{-1} between 150 and 600 °C. Data collection and analysis were performed using the STARe Software 16.00 program package.[1]

2. Computational details

Periodic density functional theory (DFT) calculations were performed using the program CRYSTAL17.[2] Crystal structures of the three cocrystal polymorphs were geometry-optimized with respect to atom coordinates and unit cell parameters, subject to the symmetry constraints of the corresponding space groups. The energies of the optimized crystal structures were used to compare the relative stability of the cocrystal polymorphs.

Electronic energies were computed with a range-separated wB97X functional[3] with a pob-TZVP triple-zeta basis set,[4] specifically adapted for periodic calculations. All-electron basis sets were used for H, C, N, O and P elements, while an effective core potential (ECP) was used for I.[5,6] The following convergence criteria were used for geometry optimization: maximum force on atom $4.5 \cdot 10^{-4}$ Ha $Bohr^{-1}$, RMS force $3.0 \cdot 10^{-4}$ Ha $Bohr^{-1}$, maximum atom displacement $1.8 \cdot 10^{-3}$ Bohr, RMS atom displacement $1.2 \cdot 10^{-3}$ Bohr. The energies of all crystal structures were corrected for basis set superposition error (BSSE) using counterpoise method with ghost atoms located up to 6 Å away from the reference molecule.

3. Preparation of the cocrystals

ortho-(**mdppo**)$_2$(**tfib**): A mixture of **mdppo** (108.1 mg, 0.5000 mmol) and **tfib** (100.5 mg, 0.2501 mmol) was placed in a PTFE jar along with a zirconia ball and 20 μL of nitromethane. The mixture was then milled for 2 or 15 min.

mono-(**mdppo**)$_2$(**tfib**): A mixture of **mdppo** (65.2 mg, 0.302 mmol), **tfib** (64.6 mg, 0.161 mmol) and 100 μL of isobutanol was briefly sonicated and then heated to obtain a clear solution, which was left to crystallize on the bench. After a few hours, the freshly formed crystals were isolated by vacuum filtration. Another route to *mono*-(**mdppo**)$_2$(**tfib**) is through thermal treatment of either the *ortho*- or the *tric*-polymorph.

tric-(**mdppo**)$_2$(**tfib**): A mixture of **mdppo** (64.9 mg, 0.300 mmol), **tfib** (60.8 mg, 0.151 mmol) and 100 μL of isobutanol was briefly sonicated and then heated to obtain a clear solution, which was left to crystallize in the freezer. After a few days, fine crystals were isolated by vacuum filtration. Alternatively, *n*-butanol can also be used in place of isobutanol, and the crystals can be harvested a day later.

4. Single crystal growth

ortho-(**mdppo**)$_2$(**tfib**): Single crystals were obtained upon evaporation of a nitromethane solution containing **mdppo** and **tfib** in a 2:1 ratio.

mono-(**mdppo**)$_2$(**tfib**) and *tric*-(**mdppo**)$_2$(**tfib**): A mixture of the single crystals of the two polymorphs were obtained upon evaporation of an acetonitrile solution containing **mdppo**, *N*,*N'*-dimethylthiourea and **tfib** in a 1:1:1 ratio.

tric-(**mdppo**)$_2$(**tfib**): Single crystals were obtained upon evaporation of an isobutanol solution containing **mdppo** and **tfib** in a 2:1 ratio.

mdppo: Single crystals were obtained upon evaporation of a nitromethane solution containing **mdppo**, **ofib** and pentafluoroiodobenzene in a 2:1:2 ratio.

5. Crystal structure determinations

The X-ray data for *mono*-(**mdppo**)$_2$(**tfib**) and *tric*-(**mdppo**)$_2$(**tfib**)@123K were collected on an Agilent SuperNova Dual diffractometer with Atlas detector using mirror-monochromatized Mo-*K*α radiation (λ = 0.71073 Å), while the X-ray data for *ortho*-(**mdppo**)$_2$(**tfib**), *tric*-(**mdppo**)$_2$(**tfib**)@253K and **mdppo** were collected on a Nonius KappaCCD diffractometer with Bruker APEX-II detector using graphite-monochromatized Mo-*K*α (λ = 0.71073 Å) radiation.

For *mono*-(**mdppo**)$_2$(**tfib**) and *tric*-(**mdppo**)$_2$(**tfib**)@123K, CrysAlisPro[7] software was used for data collection and reduction as well as applying the semi-empirical absorption correction, or numerical absorption correction based on gaussian integration in case of *tric*-(**mdppo**)$_2$(**tfib**)@123K.

For *ortho*-(**mdppo**)$_2$(**tfib**), *tric*-(**mdppo**)$_2$(**tfib**)@253K and **mdppo**, data collection and reduction were performed using the program Collect[8] and HKL Denzo and Scalepack,[9] respectively, and the intensities were corrected for absorption using SADABS,[10] except in the case of **mdppo**, where data reduction and semi-empirical absorption correction were performed using CrysAlisPro[7] software.

Structures were solved using SHELXT-2014/5[11] and refined by full-matrix least-squares on F^2 using all data, with SHELXL-2017/1[12] within OLEX2[13] and WinGX[14] packages. All non-hydrogen atoms were refined anisotropically. All carbon-bound hydrogen atoms were calculated to their optimal positions and treated as riding atoms using isotropic displacement parameters 1.2 (or 1.5 in case of methyl groups) times larger than the respective host atoms. Crystal structure figures were generated using Mercury[15] and POV-Ray.[16]

CCDC 1831924–1831928 contain the supplementary crystallographic data for this paper. The data can be obtained free of charge from The Cambridge Crystallographic Data Centre via www.ccdc.cam.ac.uk/structures.

Table S1. Crystallographic data for all the crystal structures presented in this work.

Cocrystal	*ortho*-(**mdppo**)$_2$(**tfib**)	*mono*-(**mdppo**)$_2$(**tfib**)	*tric*-(**mdppo**)$_2$(**tfib**)	*tric*-(**mdppo**)$_2$(**tfib**)	**mdppo**
CCDC Number	1831924	1831925	1831926	1831927	1831928
Formula	$C_{32}H_{26}F_4I_2O_2P_2$	$C_{32}H_{26}F_4I_2O_2P_2$	$C_{32}H_{26}F_4I_2O_2P_2$	$C_{32}H_{26}F_4I_2O_2P_2$	$C_{13}H_{13}OP$
M_r	834.27	834.27	834.27	834.27	216.20
T (K)	123.0(1)	123.0(1)	123.0(1)	253.0(1)	123.0(1)
Crystal system	orthorhombic	monoclinic	triclinic	triclinic	triclinic
Space group	*Pbca*	$P2_1/n$	$P\bar{1}$	$P\bar{1}$	$P\bar{1}$
a (Å)	5.72260(10)	11.5273(4)	6.0447(4)	6.04730(10)	8.6356(4)
b (Å)	16.3731(3)	5.88431(18)	11.5656(6)	12.0007(2)	24.2366(12)
c (Å)	32.1528(7)	23.5890(7)	12.5757(7)	12.56410(10)	16.6059(9)
α (°)	90	90	113.430(5)	116.0359(6)	90
β (°)	90	90.628(3)	100.733(5)	100.5276(7)	101.535(5)
γ (°)	90	90	97.582(5)	94.7799(7)	90
V (Å^3)	3012.61(10)	1599.95(9)	771.60(8)	791.56(2)	3405.4(3)
Z	4	2	1	1	12
ρ_{calc} (g cm^{-3})	1.839	1.732	1.795	1.750	1.265
μ (mm^{-1})	2.249	2.117	2.195	2.139	0.211
F(000)	1624	812	406	406	1368
Crystal size (mm^3)	0.23×0.18×0.14	0.400×0.290×0.148	0.334×0.174×0.138	0.35×0.31×0.30	0.42×0.27×0.09
θ range for data collection (°)	2.567–27.987	3.120–29.358	3.219–29.455	3.237–27.519	2.095–30.935
Reflections collected [R_{int}]	15206 [0.0389]	12445 [0.0258]	5563 [0.0200]	19024 [0.0253]	17889 [0.0336]
Reflections [$I > 2\sigma(I)$]	3579 [3352]	3930 [3528]	3547 [3289]	3572 [3360]	9114 [5590]
Data completeness (%)	98.6 to θ = 25.25°	99.8 to θ = 25.25°	99.2 to θ = 25.25°	99.5 to θ = 25.25°	99.6 to θ = 25.25°
Data/restraints/parameters	3579/0/192	3930/0/191	3547/0/191	3572/0/192	9114/0/409
Goodness-of-fit on F^2	1.306	1.067	1.058	1.056	1.025
Final R for data with $I > 2\sigma(I)$	R_1 = 0.0419 wR_2 = 0.1058	R_1 = 0.0227 wR_2 = 0.0454	R_1 = 0.0295 wR_2 = 0.0705	R_1 = 0.0202 wR_2 = 0.0474	R_1 = 0.0587 wR_2 = 0.1236
Final R for all data	R_1 = 0.0448 wR_2 = 0.1069	R_1 = 0.0273 wR_2 = 0.0479	R_1 = 0.0327 wR_2 = 0.0738	R_1 = 0.0222 wR_2 = 0.0482	R_1 = 0.1060 wR_2 = 0.1480
Largest diff. peak/hole (e Å^{-3})	0.701/−1.112	0.428/−0.620	1.072/−1.884	0.285/−0.363	0.539/−0.409
Extinction coefficient	0.0015(4)	-	-	0.0040(10)	-

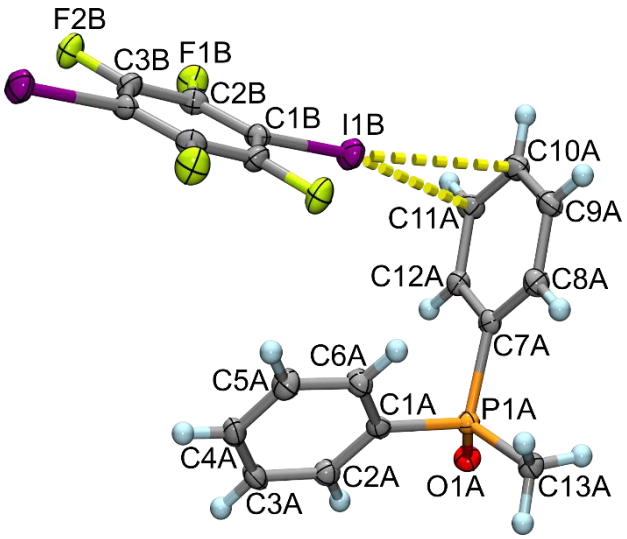

Figure S1. Asymmetric unit of *ortho*-(**mdppo**)$_2$(**tfib**), collected at 123 K, showing the atom labelling scheme. Displacement ellipsoids are drawn at the 50 % probability level, halogen bonds are marked with yellow dashed lines, and H atoms are shown as small spheres of arbitrary radius.

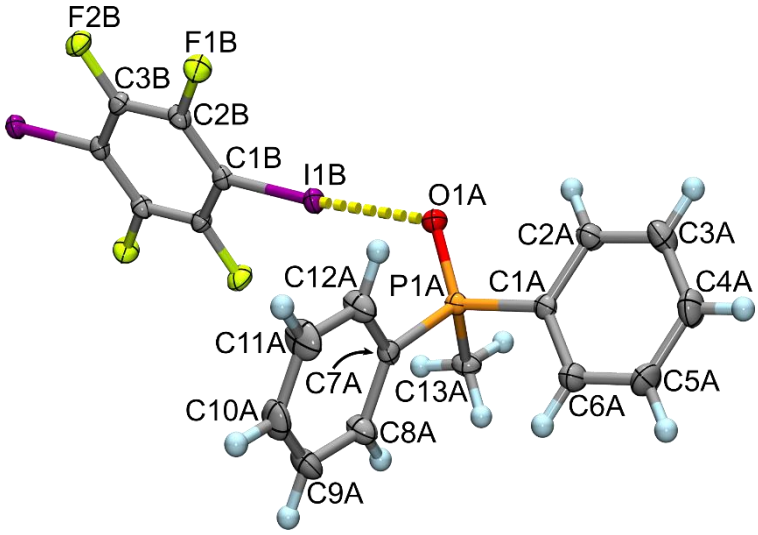

Figure S2. Asymmetric unit of *mono*-(**mdppo**)$_2$(**tfib**), collected at 123 K, showing the atom labelling scheme. Displacement ellipsoids are drawn at the 50 % probability level, halogen bond is marked with a yellow dashed line, and H atoms are shown as small spheres of arbitrary radius.

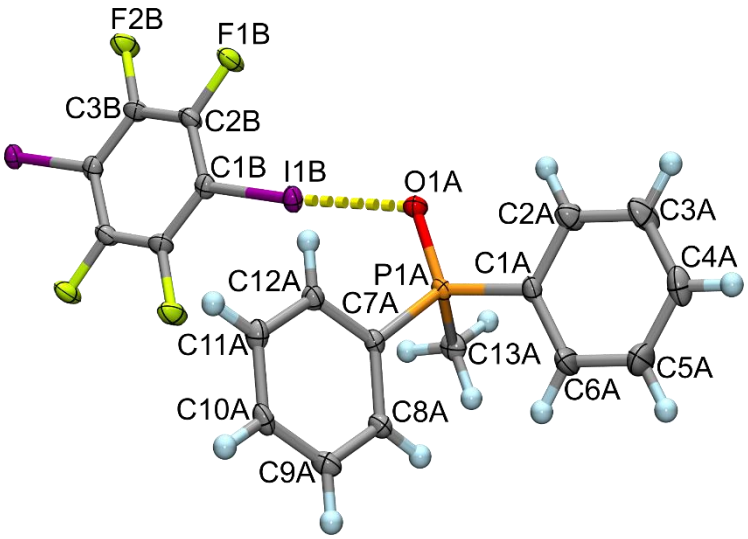

Figure S3. Asymmetric unit of *tric*-(**mdppo**)$_2$(**tfib**), collected at 123 K, showing the atom labelling scheme. Displacement ellipsoids are drawn at the 50 % probability level, halogen bond is marked with a yellow dashed line, and H atoms are shown as small spheres of arbitrary radius.

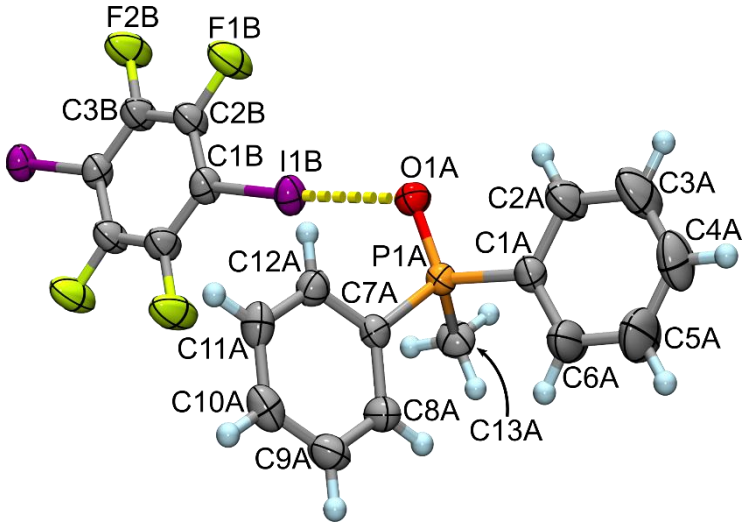

Figure S4. Asymmetric unit of *tric*-(**mdppo**)$_2$(**tfib**), collected at 253 K, showing the atom labelling scheme. Displacement ellipsoids are drawn at the 50 % probability level, halogen bond is marked with a yellow dashed line, and H atoms are shown as small spheres of arbitrary radius.

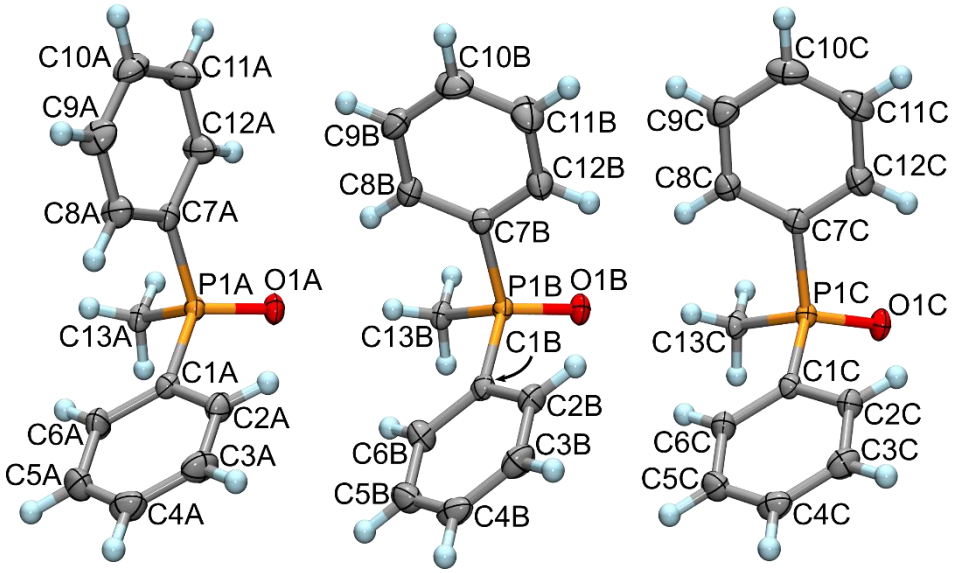

Figure S5. Asymmetric unit of **mdppo**, collected at 123 K, showing the atom labelling scheme. Displacement ellipsoids are drawn at the 50 % probability level and H atoms are shown as small spheres of arbitrary radius.

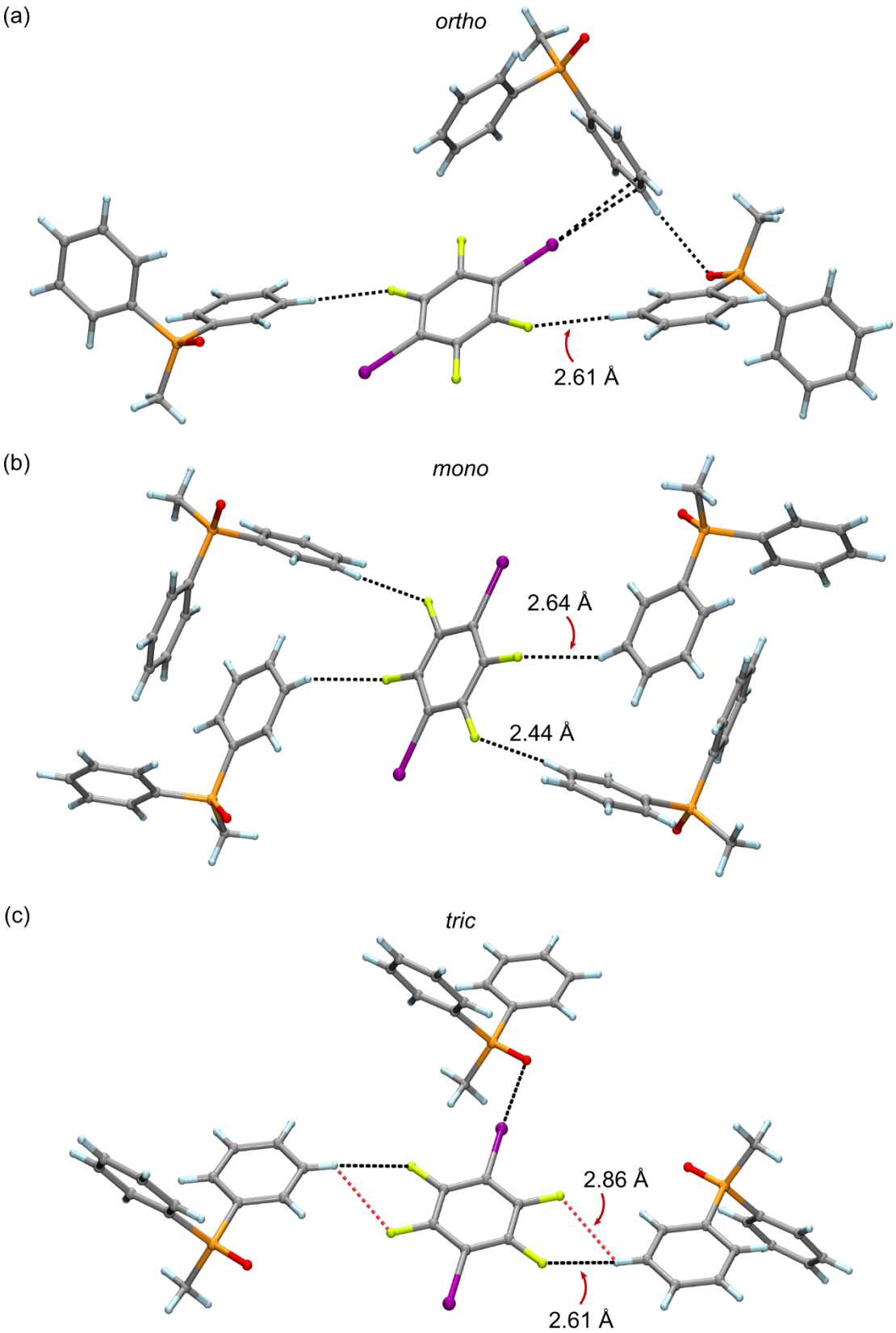

Figure S6. Short intermolecular contacts and selected distances involving **tfib** in the structures of **(a)** *ortho*-, **(b)** *mono*- and **(c)** *tric*-(**mdppo**)$_2$(**tfib**). Hydrogen (C−H···O) and halogen bonds (C−I···π and C−I···O) are omitted for clarity. Atoms are shown as spheres with radii equal to 10 % of the respective van der Waals radii. Intermolecular distances below or above the sum of the van der Waals radii are shown as dashed black or red lines, respectively.

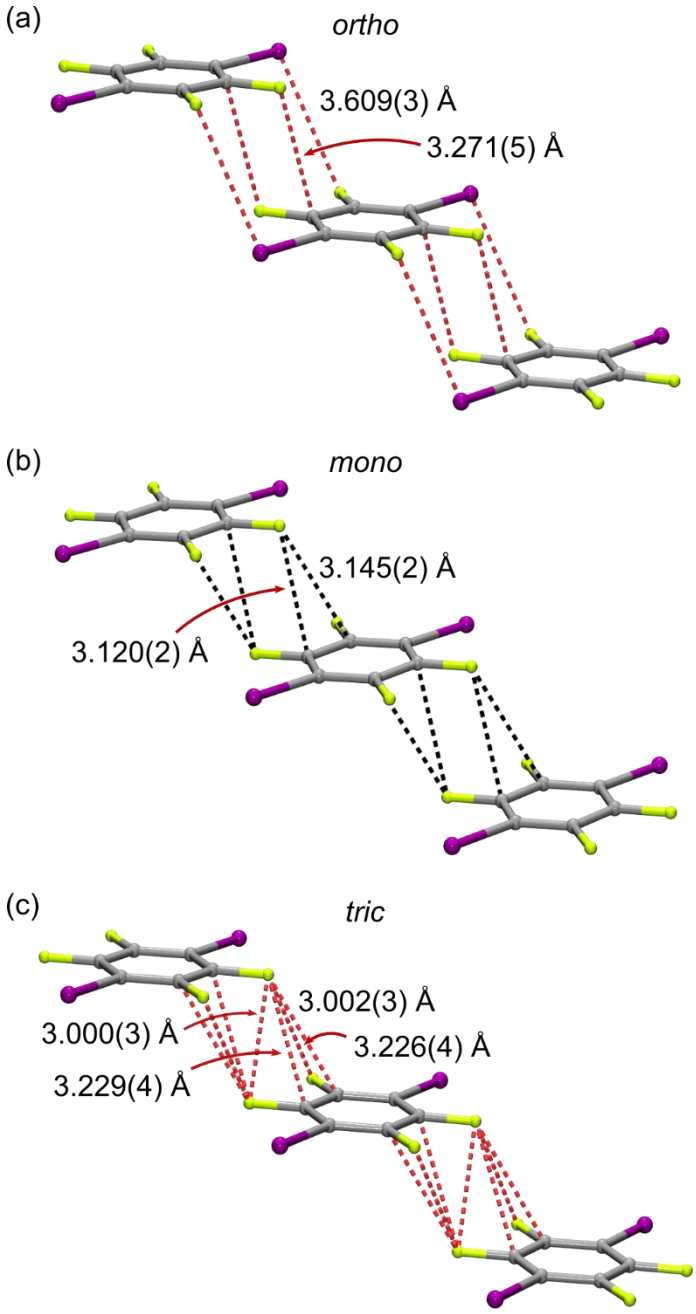

Figure S7. Short intermolecular contacts and selected distances between **tfib** molecules in the structures of **(a)** *ortho*-, **(b)** *mono*- and **(c)** *tric*-(**mdppo**)$_2$(**tfib**). Atoms are shown as spheres with radii equal to 10 % of the respective van der Waals radii. Intermolecular distances below the sum of the van der Waals radii are shown as dashed black lines, and appear only in the case of the *mono*-polymorph. However, similar structural motifs appear also in other polymorphs but in all cases with interatomic distances that are all larger than the sum of van der Waals radii, shown in red.

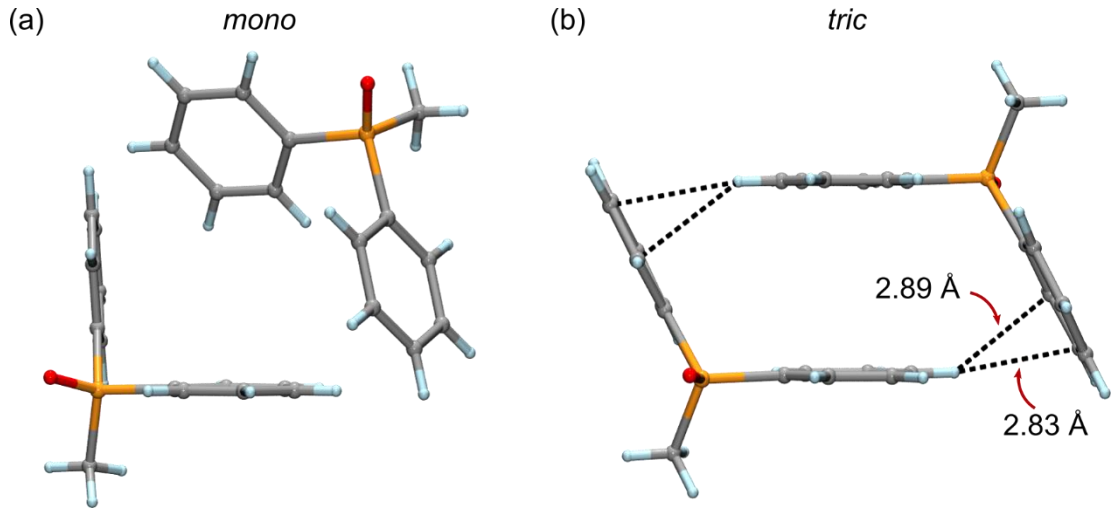

Figure S8. Short intermolecular contacts between phenyl moieties of **mdppo** molecules in the structures of **(a)** *mono*- and **(b)** *tric*-(**mdppo**)$_2$(**tfib**). Atoms are shown as spheres with radii equal to 10 % of the respective van der Waals radii. Intermolecular distances below the sum of the van der Waals radii appear only in the *tric*-form, corresponding to the four-fold embrace motif, and are shown as dashed black lines.

6. Survey of the Cambridge Structural Database

A survey of the Cambridge Structural Database (CSD version 5.40, update 1 from February 2019) based on 14 iodo- and bromoperhalogenated compounds commonly used as XB donors (Scheme S1) resulted in 984 hits. After the exclusion of datasets corresponding to pure perhalogenated compounds, majority of the remaining datasets corresponded to multi-component crystals, 936 hits. A search of these datasets for polymorphs, defined as distinct structures of identical composition revealed a total of 13 systems (1.4% of all entries for multicomponent crystals), all of which were dimorphic. No datasets were found for systems with 3 or more polymorphic forms.

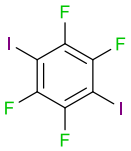

385 entries
5 dimorphic systems:
RINPOW/RINPOW01;
EWOXIZ/EWOXIZ01;
IWOMUE/IWOMUE01;
KUWPUP/KUWPUP01;
OHOWAK/OHOWAK01

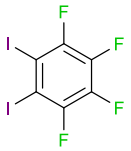

63 entries
2 dimorphic systems:
MIYKOU/MIYKOU01;
ZEBKAU/ZEBKAU01

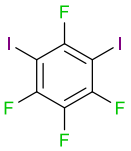

36 entries
No polymorphs
-

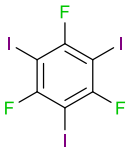

118 entries
3 dimorphic systems:
JUZRON/JUZRON01;
QECYIJ/QECYIJ01;
YAFKOI/YAFKOI01

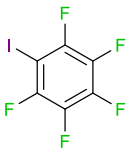

81 entries
3 dimorphic systems:
LEZPUC/LEZPUC01;
FUYFAI/FUYFAI01-
FUYFAI06;
OQIJEF/OQIXAP

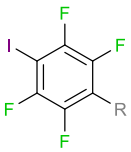

60 entries
No polymorphs
-

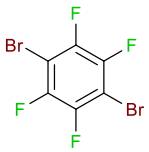

44 entries
No polymorphs
-

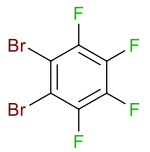

5 entries
No polymorphs
-

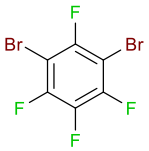

8 entries
No polymorphs

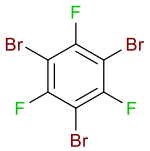

3 entries
No polymorphs

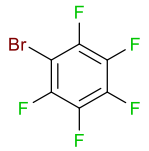

6 entries
No polymorphs

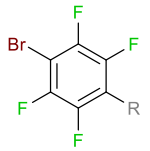

25 entries
No polymorphs

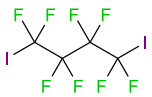

59 entries
No polymorphs

44 entries
No polymorphs

Scheme S1. Iodo- and bromoperhalogenated compounds (halogen bond donors) used for a survey of the Cambridge Structural Database (CSD). Number of entries corresponding to multicomponent crystals is shown in black and number of found polymorphic multicomponent systems is shown in red. CSD reference codes for the resulting entries are listed under the structures of respective donors.

List of CSD reference codes with respective references:

RINPOW/RINPOW01: S. d'Agostino, F. Spinelli, P. Taddei, B. Ventura and F. Grepioni, *Cryst. Growth Des.* 2019, **19**, 336–346; DOI: https://doi.org/10.1021/acs.cgd.8b01443

EWOXIZ/EWOXIZ01: R. Ramakrishnan, A. R. Mallia, M. A. Niyas, R. Sethy and M. Hariharan, *Cryst. Growth Des.* 2016, **16**, 6327–6336; DOI: https://doi.org/10.1021/acs.cgd.6b00968

IWOMUE/IWOMUE01: M. Zbačnik, M. Vitković, V. Vulić, I. Nogalo and D. Cinčić, *Cryst. Growth Des.* 2016, **16**, 6381–6389; DOI: https://doi.org/10.1021/acs.cgd.6b01037

KUWPUP/KUWPUP01: K. S. Eccles, R. E. Morrison, A. S. Sinha, A. R. Maguire and S. E. Lawrence, *Cryst. Growth Des.* 2015, **15**, 3442–3451; DOI: https://doi.org/10.1021/acs.cgd.5b00513

OHOWAK: A. Abate, S. Biella, G. Cavallo, F. Meyer, H. Neukirch, P. Metrangolo, T. Pilati, G. Resnati and G. Terraneo, *J. Fluorine Chem.* 2009, **130**, 1171–1177; DOI: https://doi.org/10.1016/j.jfluchem.2009.07.005

OHOWAK01: J. Viger-Gravel, S. Leclerc, I. Korobkov and D. L. Bryce, *CrystEngComm* 2013, **15**, 3168–3177; DOI: https://doi.org/10.1039/C3CE26750D

MIYKOU: R. Liantonio, P. Metrangolo, T. Pilati and G. Resnati, *Acta Cryst.* 2002, **E58**, o575–o577; DOI: https://doi.org/10.1107/S1600536802007201

MIYKOU01: M. B. Hursthouse, T. Gelbrich and M. J. Plater, *CSD Communication*, 2003; DOI: https://dx.doi.org/10.5517/cc7hcdg

ZEBKAU: H. D. Arman, E. R. Rafferty, C. A. Bayse and W. T. Pennington, *Cryst. Growth Des.* 2012, **12**, 4315–4323; DOI: https://doi.org/10.1021/cg201348u

ZEBKAU01: J. Viger-Gravel, J. E. Meyer, I. Korobkov and D. L. Bryce, *CrystEngComm*, 2014, **16**, 7285–7297; DOI: https://doi.org/10.1039/C4CE00345D

JUZRON: Y. Xu, J. Viger-Gravel, I. Korobkov and D. L. Bryce, *J. Phys. Chem. C*, 2015, **119**, 27104–27117; DOI: https://doi.org/10.1021/acs.jpcc.5b09737

JUZRON01: Y. Xu, J. Huang, B. Gabidullin and D. L. Bryce, *Chem. Commun.* 2018, **54**, 11041–11043; DOI: https://doi.org/10.1039/C8CC06019C

QECYIJ/QECYIJ01: I.-R. Jeon, C. Mathonière, R. Clérac, M. Rouzières, O. Jeannin, E. Trzop, E. Collet and M. Fourmigué, *Chem. Commun.* 2018, **54**, 11041–11043; DOI: https://doi.org/10.1039/C7CC03797J

YAFKOI/YAFKOI01: Y. Liu, S. Ma, B. Xu and W. Tian, *Faraday Discuss.* 2017, **196**, 219–229; DOI: https://doi.org/10.1039/C6FD00166A

LEZPUC/LEZPUC01: A. Wasilewska, M. Gdaniec, T. Połoński, *CrystEngComm*, 2007, **9**, 203–206; DOI: https://doi.org/10.1039/B617929K

FUYFAI/FUYFAI01-FUYFAI06: L. Catalano, S. Pérez-Estrada, G. Terraneo, T. Pilati, G. Resnati, P. Metrangolo and M. A. Garcia-Garibay, *J. Am. Chem. Soc.* 2015, **137**, 15386–15389; DOI: https://doi.org/10.1021/jacs.5b10776

OQIJEF/OQIXAP: F. Topić, K. Rissanen, *J. Am. Chem. Soc.* 2016, **138**, 6610–6616; DOI: https://doi.org/10.1021/jacs.6b02854

7. Variable temperature powder X-ray diffraction

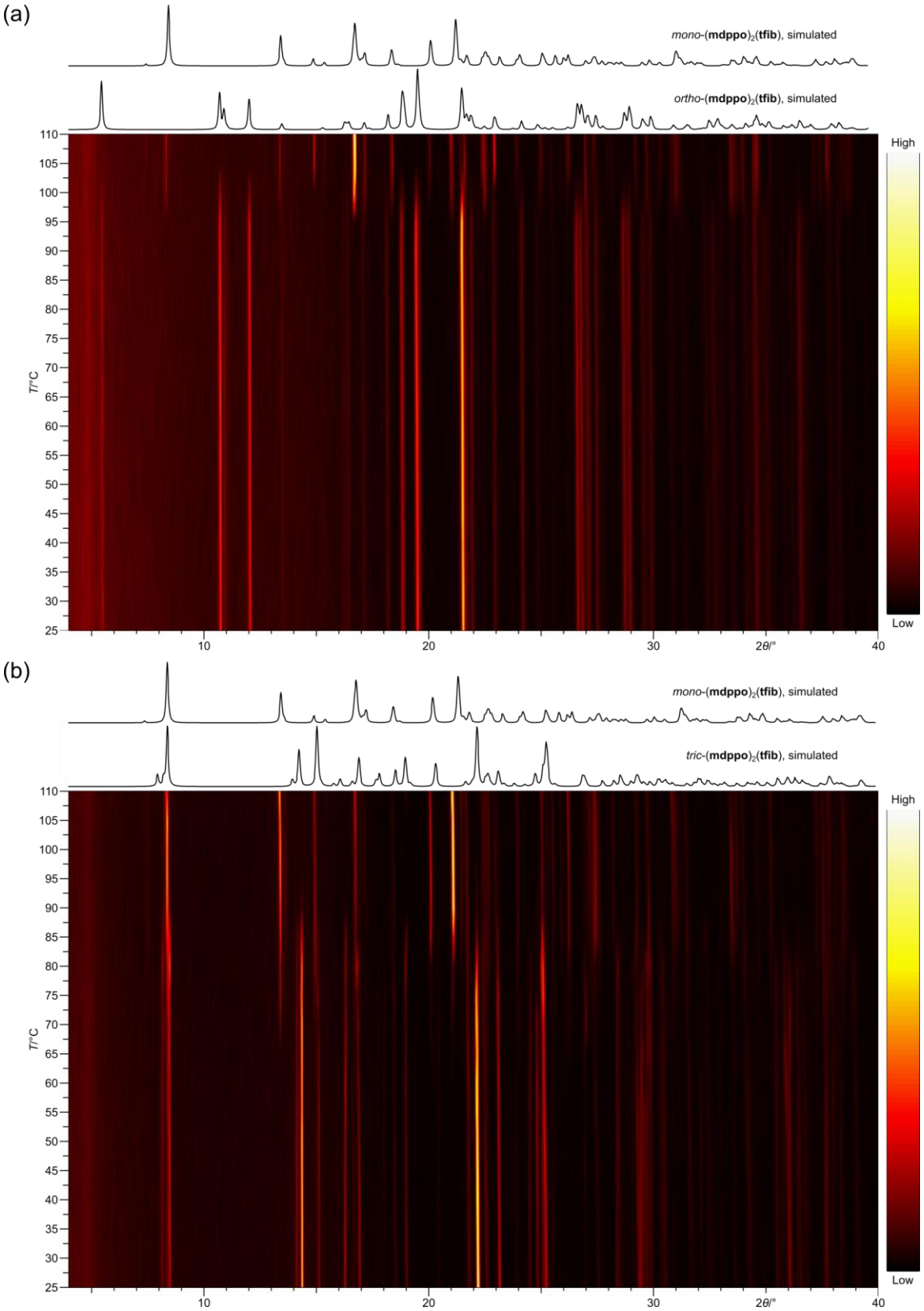

Figure S9. Variable temperature powder X-ray diffraction study of **(a)** *ortho*- and **(b)** *tric*-(**mdppo**)$_2$(**tfib**), both showing the transition into the *mono*-polymorph upon heating. In both cases the samples were heated at a rate of 5 °C/min.

8. **References**

1. STAR^e Evaluation Software 16.00, Mettler-Toledo GmbH, 1993 – 2017
2. R. Dovesi, A. Erba, R. Orlando, C. M. Zicovich-Wilson, B. Civalleri, L. Maschio, M. Rérat, S. Casassa, J. Baima, S. Salustro and B. Kirtman, *Wiley Interdiscip. Rev. Comput. Mol. Sci.*, 2018, **8**, e1360.
3. J.-D. Chai and M. Head-Gordon, *J. Chem. Phys.*, 2008, **128**, 084106.
4. M. F. Peintinger, D. Vilela Oliveira and T. Bredow, *J. Comput. Chem.*, 2013, **34**, 451–459.
5. K. A. Peterson, B. C. Shepler, D. Figgen and H. Stoll, *J. Phys. Chem. A*, 2006, **110**, 13877–13883.
6. J. Laun, D. Vilela Oliveira and T. Bredow, *J. Comput. Chem.*, 2018, **39**, 1285–1290.
7. Rigaku Oxford Diffraction, *CrysAlisPro Software system*, 2017, version 1.171.38.46, Rigaku Corporation, Oxford, UK.
8. R. W. W. Hooft, *Collect*, 1998, Nonius BV, Delft, The Netherlands.
9. Z. Otwinowski, W. Minor, *Methods in Enzymology, Macromolecular Crystallography, Part A* 1997, **276**, 307–326. Edited by C. W. Carter Jr & R. M. Sweet, New York: Academic Press.
10. L. Krause, R. Herbst-Irmer, G. M. Sheldrick, D. Stalke, *J. Appl. Crystallogr.* 2015, **48**, 3–10
11. G. M. Sheldrick, *Acta Cryst.*, 2015, A**71**, 3–8
12. G. M. Sheldrick, *Acta Cryst.*, 2015, C**71**, 3–8
13. O. V. Dolomanov, L. J. Bourhis, R. J. Gildea, J. A. K. Howard and H. Puschmann, *J. Appl. Cryst.* 2009, **42**, 339–341
14. L. J. Farrugia, *J. Appl. Cryst.* 2012, **45**, 849–854
15. C. F. Macrae, I. J. Bruno, J. A. Chisholm, P. R. Edgington, P. McCabe, E. Pidcock, L. Rodriguez-Monge, R. Taylor, J. van de Streek and P. A. Wood, *J. Appl. Cryst.*, 2008, **41**, 466–470.
16. Persistence of Vision Pty. Ltd. *Persistence of Vision Raytracer*, 2018, Persistence of Vision Pty. Ltd., Williamstown, Victoria, Australia. http://www.povray.org/